Polymer 50 (2009) 5262–5267

Contents lists available at ScienceDirect

Polymer

journal homepage: www.elsevier.com/locate/polymer

NMR quantification of the partition of coronal chain segments of block copolymer vesicles

Gabriel Njikang, Irene C.M. Kwan, Gang Wu, Guojun Liu*

Department of Chemistry, Queen's University, 90 Bader Lane, Kingston, Ontario, K7L 3N6 Canada

ARTICLE INFO

Article history:
Received 4 August 2009
Received in revised form
2 September 2009
Accepted 6 September 2009
Available online 20 September 2009

Keywords:
Block copolymer
Vesicles
T_1 relaxation

ABSTRACT

In vesicles of an ABC triblock copolymer, the soluble A and C blocks can be grafted onto the outer or the inner surfaces of the wall made of the insoluble B block. Traditionally, the determination of the fractions of A and B chain segments partitioned onto these two surfaces has been difficult. We show that they can be readily determined from NMR paramagnetic relaxation experiments. In such an experiment, a paramagnetic reagent that does not readily permeate the vesicular wall is added into a solution. This greatly shortens the spin-lattice relaxation times T_1 of these chain segments on the outer surface relative to those on the inner surface. Treating such T_1 relaxation data with a double exponential function yields the coefficients for these terms with different T_1 values and thus the relative populations for chain segments on the inner and outer vesicular wall surfaces. This method is simple and straightforward.

1. Introduction

For possible applications in controlled delivery and release [1–6], block copolymer vesicles have received much attention in the past 14 years since the seminal paper of Zhang and Eisenberg [7] on multiple morphologies of block copolymer micelles. Our literature search revealed that there have been close to 1000 publications on block copolymer vesicles [8–14]. Despite this, we are unaware of a simple technique for determining the fractions of chain segments grafted on the inner and outer surfaces of the wall of vesicles. Yet, this information is of fundamental importance in the proper understanding and proper theoretical modeling of vesicles. In the case of ABC triblock copolymer vesicles with B forming the wall and A and C forming the corona, a change in the distribution of the coronal A and C chains may change fundamentally the property and performance of the vesicles. Reported in this paper is a simple NMR technique for quantifying coronal chain segment partition in block copolymer vesicles.

In this technique, we monitor how the intensity of the ^{1}H NMR peaks of interest recovers with time after a 180° pulse to excite the spins of these protons from the normal $+z$ direction to the $-z$ direction [15]. Under normal conditions, Protons of chain segments on the inner and outer wall surfaces of a vesicle experience a similar environment and thus decay with a comparable spin-lattice relaxation time T_1. If we add into such a solution paramagnetic $Mn(EDTA)^{2-}$ and $Mn(EDTA)^{2-}$ permeates only slowly into the core of the vesicles, the concentration inside the vesicular core should be much lower than that external to the vesicle. Since the rate constant for T_1 relaxation for a chain segment is inversely proportional to the sixth power of the distance between it and a paramagnetic ion or the distance between the two magnetic dipoles [16], those chain segments on the outer surface should have a shorter T_1 than those on the inner surface. Thus, the net magnetization $M(t)$ of the spins after the initial 180° inversion pulse relaxes back with time τ to its equilibrium value M_0 following [17–19]:

$$M(\tau) = M_0\left[1 - c\left((1-p)e^{-\frac{\tau}{T_{1a}}} + pe^{-\frac{\tau}{T_{1b}}}\right)\right] \quad (1)$$

where c is a constant with a theoretical value of 2, and p, equal to M_b/M_0, is the population of chain segments in the interior of the vesicles with a longer lifetime of T_{1b}. Here M_b is the magnetization of the probed spins on the inner vesicle wall. For ^{1}H NMR, it is directly proportional to the number of protons there.

Paramagnetic ions such as Eu^{3+} and Pr^{3+} were known more than 40 years ago to complex with certain moieties and cause their NMR peaks to shift [20,21]. This phenomenon has been exploited to advantage for the study of properties of phospholipid vesicles. The resolution, immediately after the addition of paramagnetic ions, of the ^{1}H signals of the phospholipid head groups on the outer and inner vesicular wall surfaces has, for example, allowed the direct quantification of phospholipid distribution on the two sides of the vesicular walls [22]. The diffusion of such ions into the vesicular cores causes the ^{31}P or ^{1}H peaks, which are originally split

* Corresponding author.
E-mail address: gliu@chem.queensu.ca (G. Liu).

0032-3861/$ – see front matter © 2009 Elsevier Ltd. All rights reserved.
doi:10.1016/j.polymer.2009.09.016

immediately after paramagnetic ion addition, to approach and sometime to merge eventually with one another. The rate of such peak merge has thus been used to quantify the diffusion of ions across phospholid vesicle walls [23]. We could not have used the above direct technique for vesicular coronal chain distribution quantification because we did not find a paramagnetic resonance shift agent for our polymers.

While a resonance shift reagent is difficult to find, most paramagnetic species speed up the T_1 relaxation process. This effect has also been used for probing micellar properties. Kusaka et al. [24] prepared vesicles from a double-tailed surfactant with a short perfluorinated alkyl group next to its quaternary amine head. By comparing the T_1 values of the different fluorine atoms, hydrogen atoms, and the amine atom in the presence and absence of added paramagnetic species, they were able to deduce the spatial arrangement of the different groups in the vesicles. Gao et al. [25,26] used it to study the partition of compounds in the solvent phase and the core of surfactant micelles. Since the partition in such cases was dynamic or one solute molecule could be exchanged between the micellar core and the solvent phase containing a paramagnetic species many times during T_1, the net magnetization $M(\tau)$ of the spins decayed single-exponentially. A comparison of the T_1 values of the solute in solvent (water) alone and in the micellar solution allowed the quantification of the relative residence time of the solute in the solvent and micellar core phases.

Aside from NMR techniques, Luo and Eisenberg [27,28] and later Stoenescu and Meier [29] used selective fluorescence quenching to probe chain partition in vesicles. A fluorophore was placed at the junction of two blocks of a copolymer. By using quenchers that did not permeate the wall of the vesicles, they deduced, from the efficiency of fluorescence quenching, where their fluorescent tag or the tagged part of the chains was mostly located, i.e. on the inner or outer wall surface. For sufficiently small diblock copolymer vesicles, e.g. with diameter <200 nm, Luo and Eisenberg [27,28] showed that chains with a shorter soluble block segregated preferentially to the inner surface. While this technique was robust, the preparation of copolymers with a fluorophore at the junction of two blocks was nontrivial.

2. Experimental section

2.1. Materials

Methanol and methylene chloride were of reagent grade from Fisher Scientific and were used without further purification. Manganese sulfate monohydrate ($MnSO_4 \cdot H_2O$, ACS reagent, 98+%) and ethylenediaminetetracetic acid disodium salt dehydrate (EDTA, ACS reagent 99.0–101.0%) were also used as received. Pyridine (99.9%) from Fisher Scientific was dried by filtration through alumina columns of an Innovative Technology system. Trifluoroacetic acid (99%) and triethylsilane (99%) were purchased from Aldrich and were used as received. Deuterated methanol CD_3OD (99.8%) and deuterium oxide D_2O (99.9%) were from Cambridge Isotope Laboratories Inc. Paramagnetic reagent $Mn(EDTA)^{2-}$ was prepared by mixing $MnSO_4$ and EDTA at a 1/2 molar ratio in water.

2.2. Polymer

The polymer used to prepare the vesicles was poly(*tert*-butyl acrylate)-*block*-poly(2-cinnamoyloxyethyl methacrylate)-*block*-poly(monoglyceryl methacrylate) or PtBA-*b*-PCEMA-*b*-PGMA. The precursor to this polymer was prepared by anionic polymerization [30,31]. The polymer was carefully characterized by size-exclusion chromatography, light scattering, and NMR. It consisted of 110 tBA units, 195 CEMA units, and 115 GMA units and had SEC polydispersity index M_w/M_n of 1.06 [32].

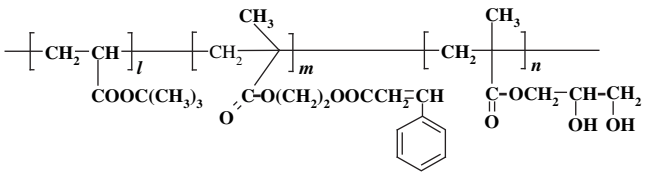

2.3. Vesicle preparation and derivatization

The vesicles were prepared by heating 40 mg of PtBA-*b*-PCEMA-*b*-PGMA in 10.0 mL of pyridine/methanol at v/v = 5/95 at 50 °C for 2 d. To lock in the vesicular structural, we took advantage of the photocrosslinking ability of the PCEMA block and irradiated the vesicles with light from a focused beam that had passed a 270 nm cutoff filter from a 500 W mercury lamp powered by an Oriel 6128 power supply. This was followed by dialysis of the resultant crosslinked vesicles against methanol to remove pyridine. The CEMA double bond conversion as determined spectrophotometrically at 280 nm was 20%.

To ensure the solubilization and thus the probing by NMR of the PtBA block in a solvent that would dissolve the paramagnetic reagent $Mn(EDTA)^{2-}$, the tBA units were hydrolyzed into poly (acrylic acid). To do this, crosslinked vesicles in methanol were concentrated and then added into diethyl ether to precipitate the vesicles. After centrifuging and decanting, the precipitate was stirred with 5 mL of diethyl ether. The dispersion was centrifuged and the supernatant was decanted. The diethyl ether rinsing procedure was repeated five times. The final precipitate was redissolved in 4 mL of methylene chloride. To the solution was then added 15 μL triethylsilane and 1.33 mL of trifluoroacetic acid to hydrolyze PtBA [31]. The mixture was stirred overnight before excess diethyl ether was added to precipitate the vesicles. The precipitate was washed thrice with diethyl ether before it was redispersed in 10 mL of methanol for storage.

2.4. Nanosphere preparation

Forty-four milligrams of PtBA-*b*-PCEMA-*b*-PSMA, where PSMA denotes poly(solketal methacrylate) [33], was dissolved in 1.5 mL CH_2Cl_2. To the solution were added 15 μL of triethylsilane and 0.75 mL of trifluoroacetic acid. The mixture was stirred for 12 h to hydrolyze PtBA. This was followed by the addition of 3 mL of a 1:1 v/v MeOH/H_2O solvent mixture and another 2 h of stirring. This led to the complete hydrolysis of PSMA. The hydrolyzed sample was dialyzed against MeOH. This yielded micelles with PAA and PGMA coronas and PCEMA cores. After dialysis, the micellar solution was photocrosslinked for 2 h to yield crosslinked spherical micelles or nanospheres.

2.5. NMR measurements

To prepare NMR samples, 1.5 mL of the vesicular solution in methanol containing about 6 mg of vesicles was transferred into a vial. The solution was then rota-evaporated. To the solid was added 0.25 mL of CD_3OD. The mixture was stirred for 6 h before the addition of 0.25 mL D_2O. The dispersion was stirred for additional 12 h before 100 μL of a $Mn(EDTA)^{2-}$ solution at concentration between 0.60 and 40.8 mM in D_2O was added. The final mixture was stirred for 10 min and then transferred into an NMR tube. Thus, the final CD_3OD to D_2O volume ratio was around 4/6. The crosslinked spherical micellar solutions were prepared analogously.

T_1 measurements were performed within 1 h after $Mn(EDTA)^{2-}$ addition. All NMR spectra were recorded on a Bruker Avance 500 MHz spectrometer (11.7 T) at 298.0 K. Chemical shifts were referenced to HDO resonance at 4.65 ppm. For ^1H experiments, the ^1H 90° pulse-width for various samples at a pulse power of 8.0 dB was between 10.5 and 12 μs. Spin-lattice relaxation times (T_1) were first estimated for each sample by finding the so-called "null" point with an inversion recovery pulse sequence (180°-τ-90°). Full T_1 measurements were subsequently carried out by using 18 random τ's. A total of 32 to 128 scans were collected for each of the 18 increment steps with a relaxation delay of 15 s. The spectral width was 6010 Hz and a total of 32,768 data points were used. Target peak intensities were extracted using NUTS V. 19990111 (1998) and plotted against τ. The relaxation data were further analyzed by a commercial software (SlideWrite®).

3. Results and discussion

3.1. Samples

The vesicle sample used in this study was prepared in pyridine/methanol at v/v = 5/95 from $PtBA_{110}$-*b*-$PCEMA_{195}$-*b*-$PGMA_{115}$, where the subscripts refer to the repeat unit numbers for the individual blocks. In such a solvent mixture, PtBA and PGMA were soluble and PCEMA was insoluble. Thus, the corona consisted of PtBA and PGMA chains.

This vesicle sample has been studied previously by transmission electron microscopy (TEM) and atomic force microscopy (AFM) [32]. Our TEM study concluded that the vesicles had a TEM diameter, including the PCEMA wall, of 116 ± 20 nm and a PCEMA wall thickness of 20 ± 2 nm. Our TEM and atomic force microscopy (AFM) and other experimental observations established that the PtBA and PGMA chains were segregated preferentially on the inner and outer wall surfaces of the vesicles, respectively [32]. The PtBA and PGMA chains were segregated because they were highly incompatible.

Fig. 1a shows an AFM phase image of the vesicles sprayed from pyridine/methanol onto silicon wafer. The bowl-shaped objects were vesicles collapsed after solvent evaporation. The round objects were the intact vesicles. On them, 19 nm dark circles were seen. These were shown from our prior TEM experiments resorting to selective staining to be PtBA patches dispersed among the PGMA chains. For NMR study, the vesicles were phololyzed to crosslink the PCEMA wall and treated with trifluoroacetic acid to hydrolyze the PtBA units into PAA units. PCEMA was crosslinked mainly to ensure the structural integrity of the vesicles during the PtBA hydrolysis step, which involved solvent changes. PtBA hydrolysis was important because PAA was soluble and PtBA was insoluble in CD_3OD/D_2O, where D_2O helped with $Mn(EDTA)^{2-}$ dissolution.

For comparison, a PCEMA-crosslinked and PtBA-hydrolyzed spherical micellar sample was also studied. The spherical micelles were prepared in methanol from PAA-*b*-PCEMA-*b*-PGMA. Shown in Fig. 1b is an AFM topography image of the nanospheres after PCEMA crosslinking. This sample had both PAA and PGMA in the corona and PCEMA in the core. Our TEM analysis indicated that the core of the micelles was 24 ± 4 nm.

3.2. T_1 measurements

Fig. 2 shows a ^1H NMR spectrum of a crosslinked PAA-*b*-PCEMA-*b*-PGMA vesicle sample at 5.0 mg/mL in CD_3OD/D_2O at v/v = 4/6. Also shown are the assignments for the different peaks. The PCEMA signals are not seen because of the low mobility of the polymer in the crosslinked wall. A similar spectrum was seen for the crosslinked spherical PAA-*b*-PCEMA-*b*-PGMA micelle sample.

For T_1 measurements, the NMR spectra were recorded at different delay times τ after the initial 180° pulse. Integrating the peaks at 3.5 ppm characteristic of PGMA and 2.3 ppm characteristics of PAA at different τ yielded the intensity-vs.-τ plots for the crosslinked vesicle sample at $[Mn(EDTA)^{2-}] = 0$, 0.10, 0.40, 3.4, and 6.4 mM, respectively. We also obtained the intensity-vs.-τ plots for the crosslinked spherical micellar sample at $[Mn(EDTA)^{2-}] = 3.4$ mM.

3.3. Data treatment and results

For data treatment our basic assumption was that T_1 did not change significantly with the location of PGMA or PAA segments in the corona in the absence of $Mn(EDTA)^{2-}$ and thus the T_1 relaxation of the PGMA and PAA chains could be described by a single exponential function. With the addition of $Mn(EDTA)^{2-}$ and for the slow diffusion of $Mn(EDTA)^{2-}$ and thus a large $[Mn(EDTA)^{2-}]$ difference across the vesicular wall, we assumed that a double exponential function was required to treat the experimental data. While only one fitting function should be chosen to treat one particular set of data, we treated each set of data using both single and double exponential functions. Results from data treatment using the more meaningful function were presented in bold in Table 1 for comparison with those obtained using the other functional form. When Eq. (1) was used, M_0, c, M_b, T_{1a}, and T_{1b} were obtained from curve fitting. Here M_0 is

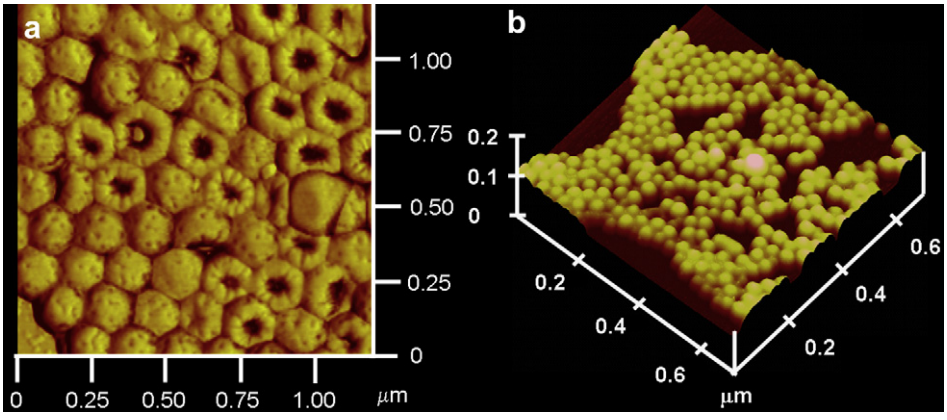

Fig. 1. AFM phase image PtBA-*b*-PCEMA-*b*-PGMA vesicles sprayed from pyridine and MeOH at v/v = 5/95 (a) and AFM topography image of PAA-*b*-PCEMA-*b*-PGMA nanospheres sprayed from MeOH (b).

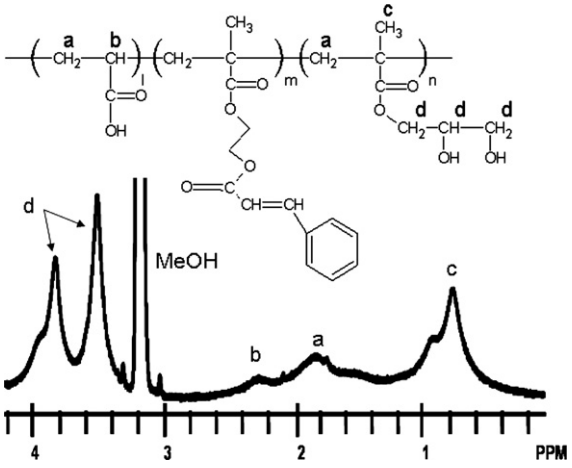

Fig. 2. Proton NMR spectra of PAA-*b*-PCEMA-*b*-PGMA vesicles at 5.0 mg/mL in CD_3OD/D_2O at v/v = 4/6.

a normalization factor and p was obtained from M_b/M_0. M_b/M_0 rather than p was used for curve fitting because the fitting program was not smart enough to recognize that p should be a fractional number less than 1. The use of a single exponential function for curve fitting yielded only the c, T_1, and M_0 values.

Also presented in Table 1 are the coefficients of determination R_v^2 for judging the quality of curve fitting [34]. A better fitting is supposed to produce a R_v^2 value closer to 1. Using this criterion we can see that the data were fitted always better by Eq. (1) than by a single exponential function with exception to two cases. This is reasonable because a double exponential function contained more fitting parameters and should to be a more robust fitting function.

The R_v^2 values from fitting data of the PAA vesicular chain segments seem to follow the expected trend exactly. In the absence of $Mn(EDTA)^{2-}$, fitting the T_1 data with a double exponential function led to no improvement in R_v^2 value relative to the case when a single exponential function was used. Also, forced fitting using a double exponential function yielded two components with the amplitude coefficient for the long-life component at 93%, which was close to 100%. Thus, a single exponential T_1 relaxation was confirmed in this case. In the presence of $Mn(EDTA)^{2-}$, data fitting by a single exponential function yielded R_v^2 values that were substantially smaller. Thus, a double exponential function was indeed required for treating the PAA T_1 relaxation data.

Unfortunately, the case for PGMA vesicular coronal segments was less clear. The R_v^2 values generated from single and double exponential fitting differed little in every case. This happened probably because T_{1b}/T_{1a} was less here than in the PAA case. With T_{1a} and T_{1b} being closer and thus more difficult to resolve and for the limited precision of the experimental data, R_v^2 values were probably a poor discriminator of theoretical models or functional forms.

A more effective method for discriminating models has been in analyzing data plotted following

$$\ln\left(\frac{M_0 - M(\tau)}{M_0}\right) = \ln c - \frac{\tau}{T_1} \quad (2)$$

Here M_0 is the magnetization at $\tau \to \infty$, and c should again be 2. Thus, a straight line should be obtained if T_1 data relax single-exponentially. Deviation from a straight line behavior indicates that a double exponential function was required to treat the data properly.

Fig. 3 shows PGMA T_1 data plotted in the $\ln((M_0 - M(\tau))/M_0)$-vs. -τ form. In the absence of $Mn(EDTA)^{2-}$, a straight line was observed. This verified our assumption that the T_1 values of PGMA segments did not change or changed little with their locations within the vesicular corona. At $[Mn(EDTA)^{2-}] = 3.4$ mM, the $\ln((M_0 - M(\tau))/M_0)$-vs. -τ plot was curved for the PGMA T_1 data. This enabled the unambiguous conclusion that a double exponential function was essential for treating the T_1 relaxation data of the vesicular PGMA segments in the presence of $Mn(EDTA)^{2-}$. Similar straight and curved plots were obtained for the T_1 relaxation data of the vesicular PAA segments in the absence and presence of $Mn(EDTA)^{2-}$. This confirmed the conclusion that we have already reached based on the R_v^2 values that the T_1 data relaxed single- and double-exponentially in these two cases.

Fig. 3 also revealed that data of PAA started to curve earlier than those of PGMA. This was reasonable because the shorter-life component should be less important for PAA because most of the PAA chains resided in the interior of the vesicles. The shorter-life component should be more important for PGMA because most of the PGMA chains were located on the exterior surface.

One may plausibly argue that $Mn(EDTA)^{2-}$ might not distribute uniformly in the outer corona of the vesicles and the observed double exponential T_1 relaxation of the vesicular coronal chains in the presence of $Mn(EDTA)^{2-}$ might be a direct result of this. To address this issue, we obtained T_1 relaxation data at $[Mn(EDTA)^{2-}] = 3.4$ mM also for the PAA-*b*-PCEMA-*b*-PGMA nanospheres. The T_1 data were also plotted in Fig. 3 in the $\ln((M_0 - M(\tau))/M_0)$-vs. -τ form. Straight lines were seen for both the PGMA and the PAA data. Furthermore, little difference was noticed in Table 1 of the R_v^2 values when a double rather than a single exponential function was used to fit the T_1 relaxation data of the spheres. Thus, these results verified unambiguously that a $[Mn(EDTA)^{2-}]$ gradient, if existed all, was too small to lead to a double exponential relaxation in the T_1 of the coronal PGMA or PAA chains of the spheres. We expect this conclusion to apply equally to the outer coronal chains of the vesicles.

Focusing on the results in bold in Table 1, we notice the following trends about the results. First, the c values were always

Table 1
Results from fitting the T_1 relaxation data of vesicles and nanospheres. The bold values except $[Mn(EDTA)^{2-}]$ concentration values were results from T_1 data treatment using the more appropriate fitting function for a given set of data.

$[Mn(EDTA)^{2-}]$ (mM)	c	T_{1a}/ms	T_{1b}/ms	T_1/ms	p	R_v
Vesicular PAA chains						
6.8	**1.80**	**30**	**600**		**71%**	**0.994**
6.8	1.69			390		0.973
3.4	**2.05**	**20**	**620**		**71%**	**0.994**
3.4	1.92			395		0.968
0.40	**2.02**	**20**	**705**		**70%**	**0.997**
0.40	1.80			455		0.964
0.10	**1.98**	**63**	**855**		**72%**	**0.997**
0.10	1.90			565		0.982
0	**1.83**			**685**		**0.998**
0	1.95	5	690		93%	0.998
Vesicular PGMA chains						
6.8	**1.85**	**120**	**740**		**18%**	**0.997**
6.8	1.90			150		0.995
3.4	**1.87**	**115**	**770**		**20%**	**0.996**
3.4	1.93			145		0.993
0.40	**1.99**	**155**	**870**		**19%**	**0.997**
0.40	2.06			200		0.995
0.10	**1.99**	**165**	**895**		**19%**	**0.997**
0.10	2.06			210		0.995
0	**1.94**			**635**		**0.997**
0	1.97	115	765		86%	0.999
PAA chains of the spherical micelles						
3.4	**2.06**			**140**		**0.994**
3.4	2.09	38	180		82%	0.995
PGMA chains of the spherical micelles						
3.4	**2.16**			**67**		**0.993**
3.4	2.21	34	98		61%	0.993

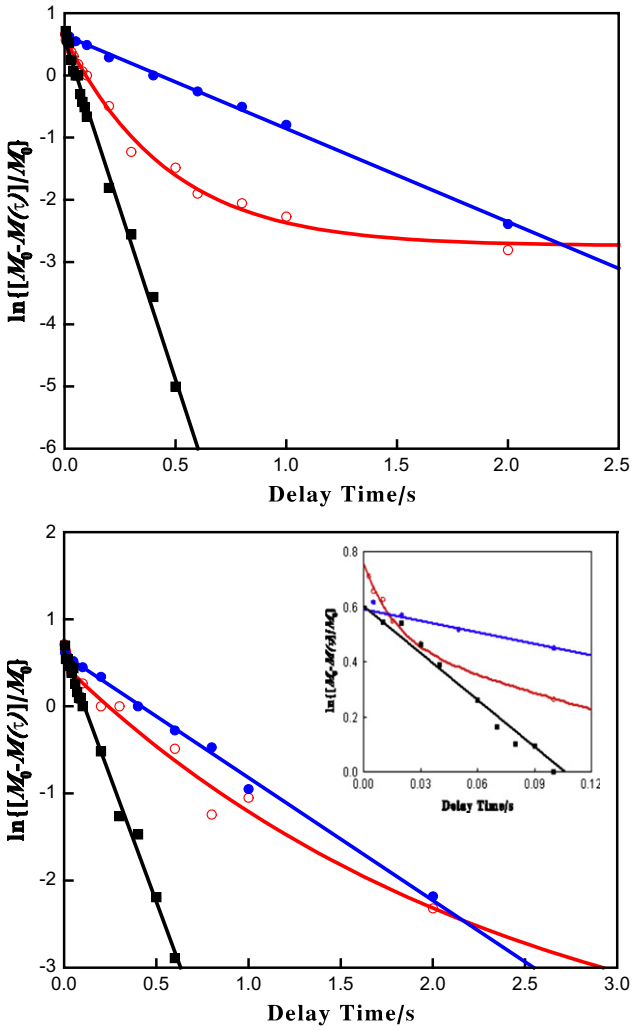

Fig. 3. Plots of $\ln((M_0 - M(\tau))/M_0)$ vs. τ for the PGMA (top) and PAA (bottom) chain segments. The symbols ●, ○, and ■ denote data for the vesicular sample in the absence of $Mn(EDTA)^{2-}$ and at $[Mn(EDTA)^{2-}] = 3.4$ mM and for the nanosphere sample at $[Mn(EDTA)^{2-}] = 3.4$ mM, respectively. The insert in the bottom figure shows data at small τ's.

~2 as expected. They deviated from 2 somewhat for errors derived from fitting the incomplete data sets with data missing at long and, in particular, at short τ's. Second, the T_{1a} and T_{1b} values of the vesicular samples decreased somewhat with increasing $[Mn(EDTA)^{2-}]$. Third, the p value or the fraction of chain segments on the inner vesicle walls was $(71 \pm 2)\%$ for PAA and $(19 \pm 1)\%$ for PGMA. Fourth, these p values changed little with $Mn(EDTA)^{2-}$ concentrations, which varied from 0.10 to 6.8 mM or by 68 times.

The decrease in T_{1a} with increasing $[Mn(EDTA)^{2-}]$ was expected because $Mn(EDTA)^{2-}$ was a "quencher".[24] The decrease in T_{1b} with increasing $[Mn(EDTA)^{2-}]$ suggests the slight "leakage" of the PCEMA wall. Fortunately, the slow permeation of the quencher into the vesicular cores should not affect, in principle, the p values determined as long as the T_{1a} and T_{1b} components remained resolved.

3.4. Accuracy of the determined p values

While we are certain about the qualitatively different behavior of the T_1 relaxation of the PGMA and PAA vesicular chain segments in the presence and absence of $Mn(EDTA)^{2-}$, a challenge has been in knowing the accuracy of the obtained p values. Here p was determined from fitting T_1 data, which consisted of a total of 18 data points with limited precision, by Eq. (1) containing 5 fitting parameters.

A convincing way to show the validity of the obtained p values would have been to obtain the p values from another technique. We attempted an analogue of the fluorescence quenching experiments used by Luo and Eisenberg [27,28]. In such an attempt, we reacted ~2 mol% of the PGMA hydroxyl groups with succinic anhydride [35,36]. The resultant carboxyl groups were then reacted with excess fluoresceinamine to graft the fluorescein groups. This was followed by the processing of the tagged polymer analogously as its untagged counterpart to yield crosslinked vesicles with PAA and PGMA coronal chains. Unfortunately, the fluorescence intensity of the sample thus obtained was too low and the scattering intensity of the vesicles was too high for any meaningful analysis to be performed. Our suspicion was that quite a fraction of the fluorescein groups was destroyed during the vesicle crosslinking and PtBA hydrolysis steps.

Without independent verification of the p values by a second technique, we still believe that the p values determined from our NMR experiments are close to their true values for the following reasons: First, the p values were determined at different $Mn(EDTA)^{2-}$ concentrations and they changed little with $[Mn(EDTA)^{2-}]$. If the p values were results of some data fitting artifacts, they should not have remained constant and independent of $[Mn(EDTA)^{2-}]$ or the experimental conditions used. Second, the p values suggest that the AA units resided mostly on the inner surface and the GMA units mostly on the outer surface of the vesicles. These were conclusions that we derived before from other experimental results. Third, the sum of the p values on the inner wall and that of the $(1 - p)$ values on the outer wall were 90% and 110%, respectively. These values are in agreement with the fact that the area of the outer surface was larger than that of the inner surface. Fourth, we have tried to reduce the number of fitting parameters from 5 to 4 by fixing M_b for treating a given set of experimental data. We then compared the c, p, T_{1a}, and T_{1b} values obtained at different inputted M_b values. This again allowed us to conclude that the p values shown in Table 1 were probably the most reasonable ones.

Table 2 shows results from fitting the T_1 relaxation data of the PGMA chain segments of the vesicles at $[Mn(EDTA)^{2-}] = 3.4$ mM using Eq. (1) at different inputted M_b values. Also shown in bold are the results obtained from fitting the data using Eq. (1) and M_b as a floating adjustable parameter. The M_b and M_0 values are dimensionless because the $M(\tau)$ values were normalized already.

While all of the R_ν^2 values were similar, the results from data fitting using M_b as a floating parameter were the most reasonable for the following reasons. First, c is close to 2 as expected. Second, T_{1b}, at 770 ms, is close to the T_1 value of 635 ms determined for PGMA segments in the absence of $Mn(EDTA)^{2-}$. The T_{1b} value should be close to 635 ms because we expected little permeation of the vesicular wall by $Mn(EDTA)^{2-}$. We think that the p value of 20% should be close to the true value because almost the same p value was obtained independent of the inputted M_b value.

Table 2
Results from fitting the T_1 relaxation data of the PGMA chain segments of the vesicles at $[Mn(EDTA)^{2-}] = 3.4$ mM using Eq. (1) at different inputted M_b values. The row of values in bold at $M_b = 0.804$ coincided with those obtained from treating the data using M_b as a floating fitting parameter.

Inputted M_b	M_0	p	c	T_{1a}/ms	T_{1b}/ms	R_ν^2
0.700	0.979	28%	1.90	100	475	0.99637
0.804	**0.999**	**20%**	**1.87**	**115**	**770**	**0.99640**
0.900	1.081	17%	1.80	125	2000	0.99637
0.950	1.187	20%	1.73	125	1750	0.99634
0.970	1.239	22%	1.70	125	4250	0.99635

Making the approximation that the PGMA and PAA chain lengths were essentially the same, we estimated from the $(1-p)$ values in Table 1 for AA and GMA segments that the AA chain segment fraction on the outer surface was ~26%. This suggested that PAA made up the minority component on the vesicular outer surface. This is in agreement with what is seen from Fig. 1a. Unfortunately, we could not quantify the fraction of PtBA segments from this AFM image for several reasons. First, the phase contrast between two polymers was very sensitive to the tapping force used during imaging [37,38], and the force used to obtain Fig. 1a was not necessarily perfectly optimized. Second, the phase segregation between the PGMA and PtBA chains might not be sharp, clean, and complete. While we had no trouble assigning the very bright and dark regions on the surface of the vesicles to the PGMA- and PtBA-rich domains, assigning the gray zones in this image involved much ambiguity.

From the p values for PAA and PGMA we calculated that PGMA made up ~21% of the chains on the inner vesicular wall. This should not be surprising. Entropy maximization should drive the uniform distribution of PGMA and PtBA onto the two surfaces. They concentrated instead onto different surfaces mainly to minimize the unfavorable PGMA and PtBA contacts. The PGMA chains were concentrated on the more spacious outer surface because it helped reduce the stretching energy of the PGMA chains [27,28]. The repulsion between the PGMA chains should be stronger than that between the PtBA chains probably for two reasons. First, the PGMA chains were slightly longer than the PtBA chains and the GMA unit was bulkier than the tBA unit. Second, the literature solubility parameters δ for pyridine and methanol are 21.9 and 29.7 $MPa^{1/2}$, respectively [39]. Our calculations based on group contributions [40,41] yielded δ values of 18.6 and 28.7 $MPa^{1/2}$ for PtBA and PGMA. These parameters indicate that PtBA should assume a less expanded conformation in the solvent mixture in which the vesicles were prepared and that consisted of pyridine/methanol with 95 vol% methanol.

4. Conclusions

In CD_3OD/D_2O at v/v = 4/6, crosslinked PAA-*b*-PCEMA-*b*-PGMA vesicles possessed a PCEMA wall and a corona made of PAA and PGMA. In the absence of $Mn(EDTA)^{2-}$, protons of the PAA or PGMA chain segments on the inner and outer wall surfaces of the vesicles had a similar spin-lattice relaxation time T_1 and could not be differentiated by NMR relaxation experiments. The addition, to such a vesicular solution, of $Mn(EDTA)^{2-}$, which permeated the PCEMA wall slowly, caused the proton spins of the chain segments on the outer surface to recover to their normal orientation much faster than those on the inner wall surface. Thus, a bi-exponential function was shown to be essential for treating the T_1 relaxation data in these cases. From the amplitude coefficients for these exponential terms, we determined that the fraction p of PAA chain segments on the inner wall surfaces was $71 \pm 2\%$ and that for the PGMA chains was $19 \pm 1\%$. These values were constant independent of $Mn(EDTA)^{2-}$ concentration. That more PGMA chain segments were on the outer wall surface and more PAA chain segments were on the inner surface was in agreement with our prior microscopy and solubility test results. The p values further suggest that there were a total of more PAA and PGMA chain segments on the outer than on the inner surface in agreement with the fact that the area of the outer surface was larger. All of the above results suggest the validity of the paramagnetic relaxation NMR technique in quantifying coronal chain segment distribution in block copolymer vesicles.

Acknowledgement

GL thanks NSERC of Canada for sponsoring this research and thanks the Canada Research Chairs program for a chair in Materials Science.

References

[1] Li MH, Keller P. Soft Matter 2009;5:927.
[2] Ding JF, Liu GJ. J Phys Chem B 1998;102:6107.
[3] Discher DE, Eisenberg A. Science 2002;297:967.
[4] Antonietti M, Forster S. Adv Mater 2003;15:1323.
[5] Discher DE, Ortiz V, Srinivas G, Klein ML, Kim Y, David CA, et al. Prog Polym Sci 2007;32:838.
[6] Onaca O, Enea R, Hughes DW, Meier W. Macromol Biosci 2009;9:129.
[7] Zhang LF, Eisenberg A. Science 1995;268:1728.
[8] Cerritelli S, Velluto D, Hubbell JA. Biomacromolecules 2007;8:1966.
[9] Ding JF, Liu GJ. Macromolecules 1997;30:655.
[10] Kukula H, Schlaad H, Antonietti M, Forster S. J Am Chem Soc 2002;124:1658.
[11] Checot F, Lecommandoux S, Gnanou Y, Klok HA. Angew Chem Int Ed 2002;41:1339.
[12] Chiu HC, Lin YW, Huang YF, Chuang CK, Chern CS. Angew Chem Int Ed 2008;47:1875.
[13] Lomas H, Canton I, MacNeil S, Du J, Armes SP, Ryan AJ, et al. Adv Mater 2007;19:4238.
[14] Zheng RH, Liu GJ. Macromolecules 2007;40:5116.
[15] Harris RB. Nuclear magnetic resonance spectroscopy: a physicochemical view. London: Pitman; 1983.
[16] Jackman LM, Sternhell S. Application of nuclear magnetic resonance spectroscopy in organic chemistry. Oxford: Pergamon Press; 1969.
[17] Tang XP, Chartkunchand KC, Wu Y. Chem Phys Lett 2004;399:456.
[18] Tang XP, Kleinhammes A, Shimoda H, Fleming L, Bennoune KY, Sinha S, et al. Science 2000;288:492.
[19] Lin WX, Zhang QJ, Yang G, Chen QJ. Mol Struct 2003;655:37.
[20] Reuben J. Paramagnetic lanthanide shift reagents in NMR spectroscopy: principles, methodology and applications. In: Emsley JWFJ, Sutchliffe LH, editors. Progress in nuclear magnetic resonance spectroscopy, vol. 9. Permamon Press; 1973. p. 1.
[21] Gupta RK, Gupta PJ. Magn Res 1982;47:344.
[22] Bergelso Ld, Barsukov LI, Dubrovin Ni, Bystrov VF. Dokl Akad Nauk SSSR 1970;194:708.
[23] Ting DZ, Hagan PS, Chan SI, Doll JD, Springer CS. Biophys J 1981;34:189.
[24] Kusaka H, Uno M, Krieg-Kowald M, Ohmachi T, Kidokoro S, Yui T, et al. Phys Chem Chem Phys 1999;1:3135.
[25] Gao ZS, Wasylishen RE, Kwak JCT. J Colloid Interface Sci 1990;137:137.
[26] Gao ZS, Wasylishen RE, Kwak JCT. J Phys Chem 1991;95:462.
[27] Luo LB, Eisenberg A. Langmuir 2001;17:6804.
[28] Luo LB, Eisenberg A. J Am Chem Soc 2001;123:1012.
[29] Stoenescu R, Meier W. Chem Commun 2002:3016.
[30] Liu GJ, Yan XH, Li Z, Zhou JY, Duncan S. J Am Chem Soc 2003;125:14039.
[31] Yan XH, Liu GJ, Li Z. J Am Chem Soc 2004;126:10059.
[32] Njikang G, Han DH, Wang J, Liu GJ. Macromolecules 2008;41:9727.
[33] Liu FT, Liu GJ. Macromolecules 2001;34:1302.
[34] Graybill FA. Regression analysis: concepts and applications. Belmont, Calif: Duxbury Press; 1994.
[35] Li Z, Liu GJ, Law SJ, Sells T. Biomacromolecules 2002;3:984.
[36] Koh K, Liu GJ, Willson CG. J Am Chem Soc 2006;128:15921.
[37] Magonov SN, Elings V, Whangbo MH. Surf Sci 1997;375:L385.
[38] Wang J, Horton JH, Liu GJ, Lee SY, Shea KJ. Polymer 2007;48:4123.
[39] Brandrup J, Immergut EH. Polymer handbook. 3rd ed. New York: John Wiley & Sons; 1989. p. VII 3.
[40] Hu JW, Njikang G, Liu GJ. Macromolecules 2008;41:7993.
[41] van Krevelen DW. Properties of polymers–their correlation with chemical structure; their numerical estimation and prediction from additive group contributions. 3rd ed. Amsterdam: Elsevier Science; 1997.